SIMULATION STUDIES OF COLLISION CASCADES IN LIQUID In TARGETS*

D. Y. LO, M. H. SHAPIRO**, and T. A. TOMBRELLO

Division of Physics, Mathematics, and Astronomy, 301-38
California Institute of Technology,
Pasadena, California 91125

and

B. J. GARRISON and N. WINOGRAD

Department of Chemistry
Pennsylvania State University
University Park, Pennsylvania 16802

ABSTRACT

Multiple interaction computer simulations have been used to determine the properties of collision cascades in liquid In targets induced by normally incident 5 keV Ar^+ ions. Below the first atomic layer the cascade becomes Thompson-like relatively quickly. However, within the first atomic layer the angular distribution of moving atoms became forward peaked by 150 fs and remained so until $\sim$300 fs. Energy and angle resolved (EARN) spectra were calculated for the ejected atoms. The peak of the energy distribution shifted to lower energies at larger ejection angles, and the angular distributions became broader for lower energy particles. Both results agree with recent experimental data, and with a simple model proposed by Garrison. Our results suggest that the detailed structure of the surface layer is very important in the sputtering process.

To appear in the Proceedings of the Materials Research Society Meeting, Boston, 1986.

*Supported in part by the National Science Foundation [DMR83-06541 at Caltech and DMR83-06548 at California State University, Fullerton].
**Permanent address: Dept. of Physics, Calif. State Univ., Fullerton, CA 92634.

ONE OF THE BROWN BAG PREPRINT SERIES
IN BASIC AND APPLIED SCIENCE

January 1987

INTRODUCTION

In Thompson's model of sputtering [1] the distribution of ejected atoms is given by

$$\frac{d^2N(E,\theta)}{dEd\Omega} = \frac{AE\cos\theta}{(E+U)^{n+1}} \qquad (1)$$

where n depends on the atomic cross section and the nature of the collision cascade inside the target, U is the energy cost [2] to remove an atom from the surface, and A is a normalization constant. Deviations from the pure $\cos\theta$ dependence have been observed in previous experiments and simulations [3,4]. Energy distributions are well described by (1) if U and n are considered free parameters, although U is close to the cohesive energy and n is near 2. The energy and polar angle dependencies are decoupled completely in (1). However, recent energy and angle resolved neutral atom (EARN) spectra of ejected atoms show a shift towards lower energy for the peak in the energy distribution as the polar angle becomes more grazing, and a broadening of the polar angle distribution with decreasing energy [5].

Garrison [6] has proposed a modified version of (1) to fit the EARN data, namely:

$$\frac{d^2N(E,\theta)}{dEd\Omega} = \frac{AE\cos\theta}{(E+U)^{m/2+n+1}}\{U+E\cos^2\theta\}^{m/2} \qquad (2)$$

This formula with its additional free parameter m adequately predicts both the peak position shift in the energy distribution and polar angular distribution broadening. The parameters m and n depend on the nature of the collision cascade inside the target. (1) results from Thomson's assumption of an isotropic velocity distribution inside the target, while Garrison made the *ad hoc* assumption of a $\cos^m\theta$ velocity distribution within the target.

Our simulation studies are aimed at determining the nature of the velocity distribution within a liquid In target. However, on the time scale for the development of a collision cascade (a few hundred femtoseconds) the target can be considered an amorphous solid. Thus, our results should

be comparable to those from polycrystalline targets.

The decoupling of angle and energy variables in (1) results from the assumption of an isotropic flux

$$\Phi_i(E_i,\theta_i)dE_i d\Omega_i \propto \frac{1}{E_i^n}\frac{dE_i d\Omega_i}{4\pi} \tag{3}$$

inside the target. (The subscript i denotes variables inside the target.) To obtain the distribution of ejected atoms, the flux perpendicular to the surface is taken and subjected to the variable transformation $E_i \rightarrow E$ and $\theta_i \rightarrow \theta$ where E and θ are the energy and polar angle measured outside the range of a planar surface potential. Equation (1) then is obtained from

$$\frac{d^2N}{dE d\Omega} = \Phi_i(E_i,\theta_i)\cos\theta_i \frac{dE_i d\Omega_i}{dE\, d\Omega} dE d\Omega, \tag{4}$$

with $\Phi_i(E_i,\theta_i)$ as given by (3). Garrison assumed an anisotropic flux [6]

$$\Phi_i(E_i,\theta_i)dE_i d\Omega_i \propto \frac{\cos^m\theta_i}{E_i^n} dE_i d\Omega_i. \tag{5}$$

Since E_i and θ_i are still decoupled equation (2) can be obtained from (4).

The energy distribution integrated over the hemisphere then is

$$\frac{dN(E)}{dE} = \frac{\pi A}{b}\frac{1}{(E+U)^a}\{(U+E)^b - U^b\}, \tag{6}$$

where $a = (m/2)+n+1$ and $b = (m/2)+1$. This energy distribution has a single peak at $E_p = U\{(a/n)^{1/b} - 1\}$. Careful examination of (2) reveals that while the peak position in the energy distribution for a particular angle depends on n and is proportional to E, the separation between energy peak positions for different angles depends strongly on m. Peak positions generally decrease with n and their separations generally increase with m.

SIMULATION MODEL

The multiple interaction (MI) code SPUTI [7] was used for this study. Liquid targets consisting of 603 In atoms melted from a fcc structure and heated to a temperature of ~900 K [8] were bombarded with normally incident 5 keV Ar ions. Different liquid targets were generated by modeling the In target without the ion beam present. Atom velocities and positions were stored every picosecond, and the resulting target was used for 25 ion impacts at different locations. Each target was restored to its initial state before each impact in order to simulate the experimental conditions in [5] where the dose was very low. A total of 1000 impacts on 40 different targets were computed on the California State University Cyber-760 computer system.

Pair-wise additive potentials were assumed in the study. The atom-atom potential consisted of a Moliere core joined to a Morse well with a cubic spline. The ion-atom potential was a simple Moliere. Potential parameters were obtained by standard procedures [9-11]. The form of the potentials and the associated parameters are given in Table 1.

Table 1
Potential Parameters

Ion-atom

$V_{ij} = (A/r)[0.35e^{-0.3r/B} + 0.55e^{-1.2r/B} + 0.1e^{-6r/B}]$ $\quad r < r_a$

$V_{ij} = 0$ $\quad r \geq r_a$

$A = 12701.\ eV\,Å \quad B = 0.09335\,Å \quad r_a = 2.868\,Å$

Atom-atom

$V_{ij} = (A/r)[0.35e^{-0.3r/B} + 0.55e^{-1.2r/B} + 0.1e^{-6r/B}]$ $\quad r < r_a$

$V_{ij} = C_0 + C_1 r + C_2 r^2 + C_3 r^3$ $\quad r_a \leq r < r_b$

$V_{ij} = D_e[e^{-2b(r-r_e)} - 2e^{-b(r-r_e)}]$ $\quad r_b \leq r < r_c$

$V_{ij} = 0$ $\quad r \geq r_c$

$A = 34574.\ eV\,Å \quad B = 0.08065\,Å \quad C_0 = 89.151\ eV \quad C_1 = -23.619\ eV/Å$

$C_2 = -33.167\ eV/Å^2 \quad C_3 = 11.797 eV/Å^3 \quad D_e = 0.343\ eV \quad b = 1.014\,Å^{-1}$

$r_e = 3.447\,Å \quad r_a = 1.88\,Å \quad r_b = 2.04\,Å \quad r_c = 4.71\,Å$

RESULTS

Energy and polar angular distributions of ejected atoms were angle and energy resolved, respectively. Energy distributions were obtained for angular intervals of 0^0 to 30^0, 30^0 to 60^0, and 60^0 to 90^0. Polar angular distributions were obtained for energy intervals of 0 to 2 eV, 2 to 4 eV, and 4 to 6 eV (figs. 1 and 2). The peak positions of the energy distributions clearly exhibit a shift toward higher energieswith decreasing polar angles, while the polar angular distributions broaden with lower energies. These trends basically agree with the experimental EARN data [5] and the predictions of Garrison [6]. The distributions predicted by (2) with m = 2.22, n = 2.07, and U = 1.98 eV are shown in figs. 1 and 2 for comparison. The parameters m, n, and U were obtained by fitting the simulated angle-integrated energy distributions to (6). This resulted in a simulated angle-integrated energy distribution peak at 0.8 eV in comparison to the experimentally observed value of ~2 eV [5].

The energy and polar angular distributions of atoms with kinetic energy > 1 eV in the first and second surface layers of the target were sampled at various times throughout the collision cascade. The 1 eV cut-off excluded most of the atoms outside the collision cascade. The first layer distributions were fitted to the anisotropic flux of (3) which was assumed by Garrison. Since $d^2N_i/dE_i d\Omega_i = (2mE_i)^{-1/2}\,\Phi_i(E_i,\theta_i)$, dN_i/dE_i was fitted to $A/E^{n+1/2}$ while $dN_i/d\Omega_i$ was fitted to $B\cos^m\theta + C$ where A, B, and C are constants. The finite bin size of the simulated distributions was accounted for by integrating the analytical expressions over each bin before fitting. All fitting was done by minimizing χ^2 assuming that the uncertainty in the simulated distributions was governed by a Poisson distribution. The resulting values of m and n are tabulated in Table 2. The small values of χ^2_υ are an indication that Poisson statistics over-estimates the uncertainties in the simulated spectra.

Table 2
First Layer Flux Distribution Parameters

Time (fs)	m	χ^2_υ	n	χ^2_υ
100	0.52 (.25)*	0.38	0.67 (.17)*	0.47
150	1.4 (.65)	0.38	0.75 (.10)	0.42
200	1.1 (.27)	0.30	1.0 (.10)	2.2
250	1.5 (.42)	0.65	1.4 (.10)	3.8
300	1.1 (.35)	0.63	1.8 (.12)	2.3
400	0.46 (.22)	0.56	2.4 (.21)	1.8

***The quantities in parenthesis are the expected statistical uncertainties assuming a Poisson distribution.**

The first layer angular distribution shows a definite forward peak by 150 fs and becomes nearly isotropic by 400 fs (Table 2 and fig. 3). The greatest anisotropy occurs at ~250 fs. This should be the most important distribution since all sputtered atoms must traverse the first layer, and most atoms are ejected near this time in the cascade development. The second layer angular distribution is isotropic from 100 to 300 fs, then becomes transversely peaked by 400 fs. This may be an artifact of the finite size and slab-like geometry of the target. The energy distribution parameter n increases monotonically with time and has roughly the same value for the first and second atomic layers. This reflects the steady degradation in average energy of the atoms as the collision cascade ages.

DISCUSSION

Our results show that the presence of a free surface (neglected in the Thompson model) causes significant anisotropy in the first layer flux. This anisotropy diminishes quickly in the subsurface layers. The strong anisotropy in the surface layer portion of the collision cascade occurs at the time when the greatest number of atoms are ejecting. This has significant effects on the sputtered atom distributions. These effects have been seen both in recent experiments and the present simulations.

It is clear from our simulation that both the peak position shift in the energy distribution and the broadening of the angular distributions can be explained using pairwise interactions of the target atoms. However, the

large discrepency between the energy peak position in the simulated spectra (0.8 eV), and the experimental value (~2 eV) may reflect some inadequacy in the pair potential model. Studies which include many body effects through the use of an effective medium model are now underway [12].

References

1. M.W. Thompson, Phys. Rept. 69, 337 (1981).
2. B.J. Garrison, N. Winograd, D.Y. Lo, T.A. Tombrello, M.H. Shapiro, and D.E. Harrison Jr., Surf. Sci. (1986) in press.
3. M.F. Dumke et al., Surf. Sci. 124, 407 (1983).
4. M.H. Shapiro, D.Y. Lo, P.K. Haff and T.A. Tombrello, NIM B13, 348 (1986).
5. J.P. Baxter, J. Singh, G.A. Schick, P.H. Kobrin, and N. Winograd, NIM B17, 300 (1986).
6. B.J. Garrison, NIM B17, 305 (1986).
7. M.H. Shapiro, Technical Rept. 88-1 Caltech (1983).
8. D.Y. Lo, T.A. Tombrello and M.H. Shapiro, NIM B17, 207 (1986)
9. I.M. Torrens, Interatomic Potentials, (Academic Press, New York, 1972).
10. L.A. Girifalco and V.G. Weizer, Phys. Rev. 114, 687 (1959).
11. C. Kittel, Introduction to Solid State Physics, 5th ed. (Wiley, N.Y., 1976).
12. B.J. Garrison, N. Winograd, D.Y. Lo, T.A. Tombrello, M.H. Shapiro, and D.E. Harrison, Jr., in preparation.

Figure Captions

Fig. 1 Angle resolved energy spectra. The solid lines are fits to Garrison's empirical formula [6].

Fig. 2 Energy resolved angular distributions. The solid lines are fits to empirical formula [6].

Fig. 3 Time development of first layer angular distributions.

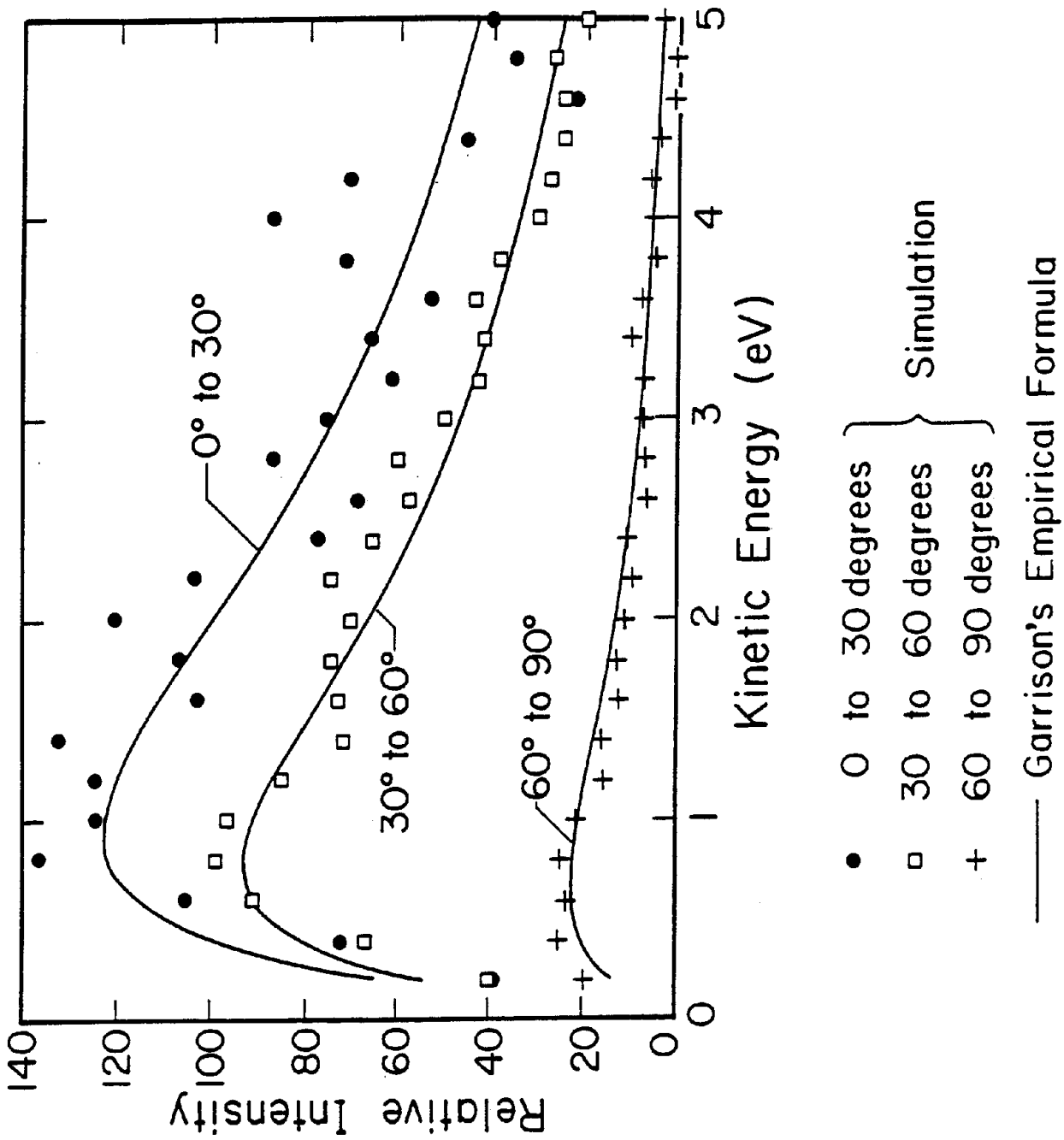
Relative Intensity
Kinetic Energy (eV)
0° to 30°
30° to 60°
60° to 90°
0 to 30 degrees
30 to 60 degrees
60 to 90 degrees
Simulation
Garrison's Empirical Formula

Fig. 1

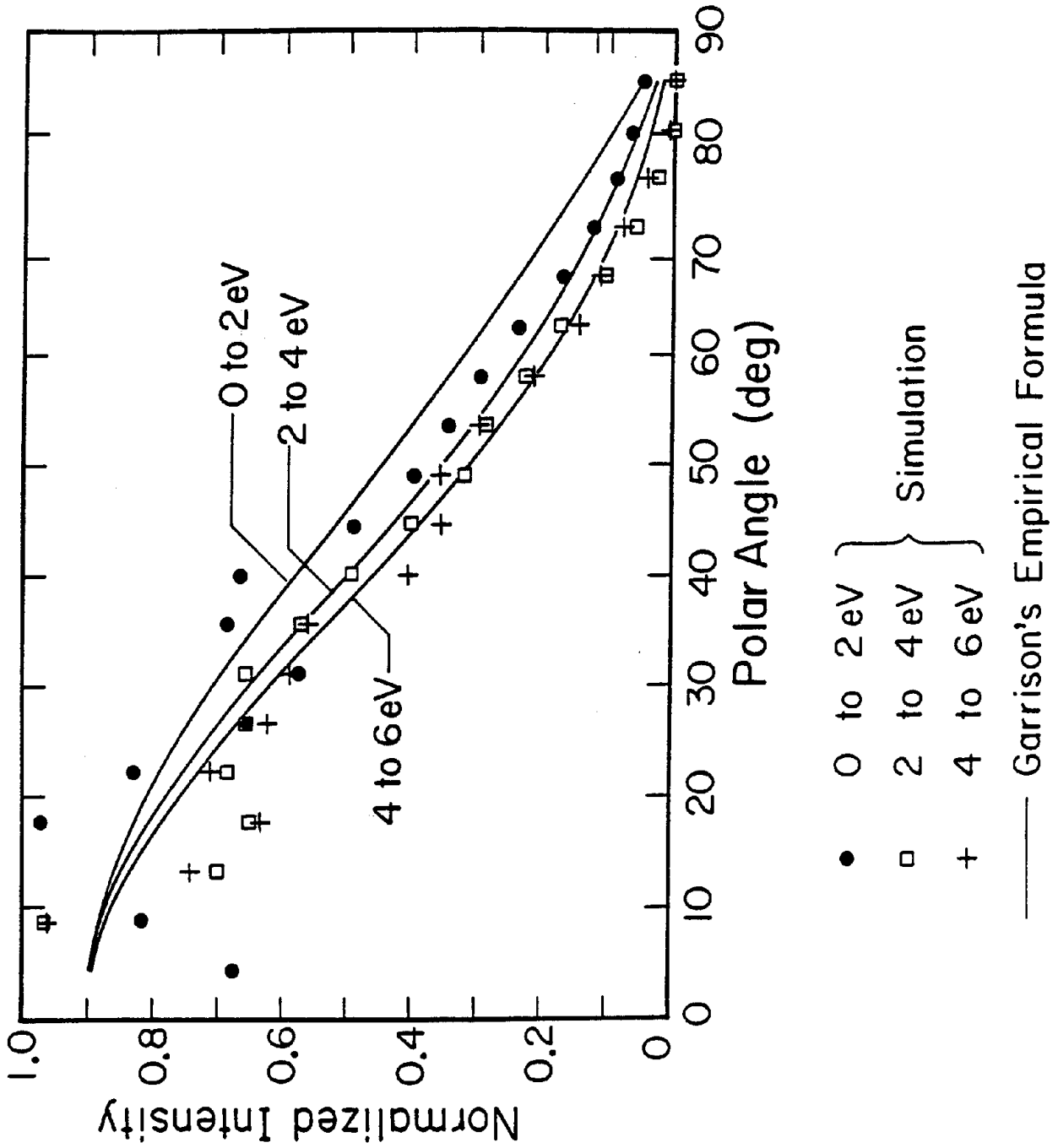
Normalized Intensity
1.0
0.8
0.6
0.4
0.2
0
0
10
20
30
40
50
60
70
80
90
Polar Angle (deg)
0 to 2eV
2 to 4 eV
4 to 6eV
0 to 2eV
2 to 4eV
4 to 6eV
Simulation
Garrison's Empirical Formula

Fig. 2

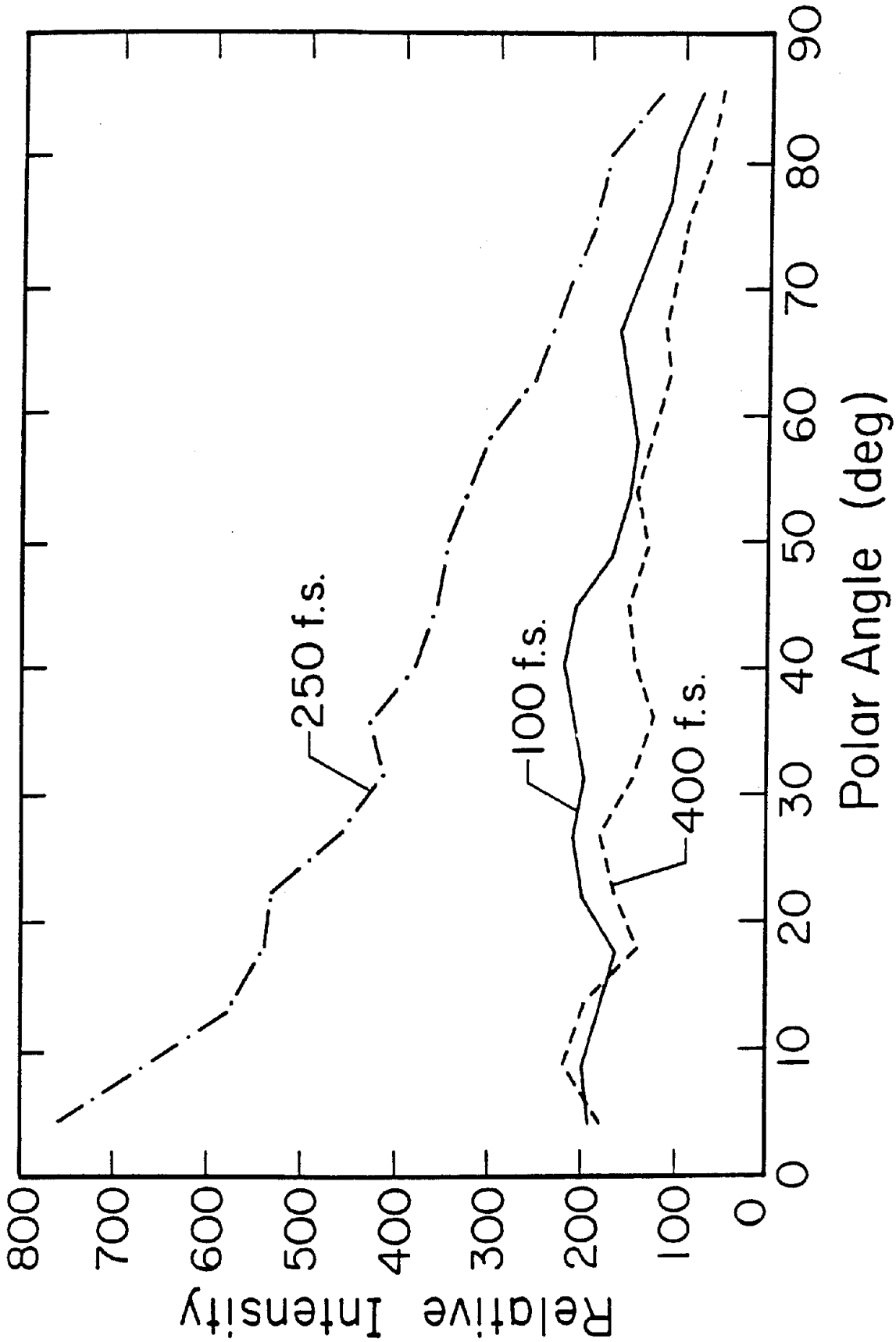
Relative Intensity
800
700
600
500
400
300
200
100
0
0
10
20
30
40
50
60
70
80
90
Polar Angle (deg)
250 f.s.
100 f.s.
400 f.s.

Fig. 3

BROWN BAG PREPRINT SERIES

BB-35 Ionizing Beam-Induced Adhesion Enhancement and Interface Chemistry for Au-GaAs
BB-36 The Grain-Bed Impact Process in Aeolian Saltation
BB-37 Liquid Target Generation Techniques in Molecular Dynamics Studies of Sputtering
BB-38 The Measurement of Eolian Sand Ripple Cross-Sectional Shapes
BB-39 Booming Dunes
BB-40 Dynamical Simulations of Granular Materials Using Concurrent Processing Computers
BB-41 A Simulation Study of the Low Energy Ejecta Resulting from Single Impacts in Eolian Saltation
BB-42 Particles in Motion: The Case of the Loaded Die
BB-43 Comparison of Several Nuclear Reaction Techniques for Hydrogen Depth Profiling in Solids
BB-44 Surface Cracking of Vitreous Fused Silica Induced by MeV Ion Beam Bombardment
BB-45 Computer Simulation of the Mechanical Sorting of Grains
BB-46 Feedback in Wind-Blown Sand Transport
BB-47 Scratching the Surface
BB-48 Computing with Particles
BB-49 Faunal Sorting of Sediments: Some Experiments with Desert Beetles Genus (Eleodes)
BB-50 The Impact Process in Eolian Saltation: Two-Dimensional Studies
BB-51 The Ubiquity of C-H Bond Breaking by MeV Ion Irradiation
BB-52 Electrical and Structural Changes in GaAs Crystals from High-Energy, Heavy-Ion Implants
BB-53 Hydrogen Depth Profiling in Solids: A Comparison of Several Resonant Nuclear Reaction Techniques
BB-54 Response of Desert Pavement to Surface Disturbances